Author postprint of the paper published in
Journal of Magnetism and Magnetic Materials 352 (2014) 6–12

Magnetocaloric effect of monovalent K doped manganites $Pr_{0.6}Sr_{0.4-x}K_xMnO_3$ (x = 0 to 0.2)

R. Thaljaoui [a,b,c], W. Boujelben[a], M. Pękała[c], K. Pękała[b], J.-F. Fagnard[d], P. Vanderbemden[d], M. Donten[c]. A. Cheikhrouhou[a].

(a) Laboratoire de Physique des Matériaux, Faculté des Sciences de Sfax, Université de Sfax, B. P. 1171, 3000 Sfax, Tunisia.
(b) Faculty of Physics, Warsaw University of Technology, Koszykowa 75, 00-662 Warsaw, Poland.
(c) Department of Chemistry, University of Warsaw, Al. Zwirki i Wigury 101, 02-089, Poland.
(d) SUPRATECS, Department of Electrical Engineering and Computer Science (B28), University of Liege, Belgium.

Abstract
Magnetic and magnetocaloric properties are reported for polycrystalline monovalent potassium doped manganites $Pr_{0.6}Sr_{0.4-x}K_xMnO_3$ (x = 0, 0.05, 0.1, 0.15 and 0.2) crystallized in orthorhombic structure with Pnma space group. The increasing K content shifts the paramagnetic to ferromagnetic transition temperature from 310 K for x = 0 to 269 K for x = 0.2. The magnetic entropy change under magnetic field variation of 2T is found to be 1.95, 3.09, 2.89, 3.05 and 3.2 $Jkg^{-1}K^{-1}$for x varying from 0 to 0.2, respectively. The highest relative cooling power of 102 J/kg is observed for the undoped sample. The sensitivity of magnetic entropy change to magnetic field is estimated by a local N(T) exponent exhibiting the characteristic temperature variation. Phenomenological universal curves of entropy change and Arrott plots confirm the second order phase transition.

Introduction

The magnetocaloric effect, known for more than 130 years, has been used for a long time to achieve the lowest temperatures. Fifteen years ago the discovery of giant magnetocaloric effect near room temperature has launched considerable interest and hope for practical applications in refrigerating systems competitive to traditional gas compression / expansion refrigerators [1]. However, the giant magnetocaloric effect (MCE) is observed only in a few materials with strong coupling between magnetic and lattice systems leading to first order magnetic phase transition entangled with structural changeover occurring in relatively narrow temperature interval. Since these systems contain expensive elements, like Gd, there is a search for alternative materials. It was found that several mixed valence manganites substituted on A site, exhibit the weaker magnetocaloric effect spread over a broader temperature interval, which may offer enough cooling power. Moreover, the manganites can be easy manufactured, are stable and cheap. Besides the possible technological applications the magnetocaloric studies enable the basic insight into the nature of the phase transitions. The selected manganites revealing a strong MCE, still remain the promising candidates for magnetic refrigerating systems and require additional complementary characterization.

The manganites are well known to exhibit the transition from the paramagnetic insulator to ferromagnetic metallic with colossal magnetoresistive (CMR) behavior. This phenomenon has been explained on the basis of Zener double exchange theory involving the mobile electrons e_g traveling between the Mn^{3+} and Mn^{4+} cations [2, 3]. Further investigations have confirmed that other factors such as ionic size mismatch, bond length Mn-O and bond

angle Mn-O-Mn, strongly affect physical properties [4, 5]. Several authors have reported that the substitution in the A sites by divalent elements (Ba, Ca) can improve physical properties [6, 7], since the addition of the divalent e.g. Sr^{2+} converts the antiferromagnetic insulating $PrMnO_3$ to the metallic $Pr_{0.6}Sr_{0.4}MnO_3$ ferromagnet. Recently the new investigation field is focused on the manganites doped with monovalent elements, like Na, K, Li and Ag [8-10]. Monovalent elements are known to convert twice more Mn^{3+} to Mn^{4+} ions as compared to divalent ones [11]. Moreover, the crystal structure may be modified depending on the radius of monovalent ions. This in turn affects the effective magnetic interaction. It was also observed that the charge ordering appears for some doping limit, e.g. in $Pr_{0.8}Na_{0.2}MnO_3$ manganites [12].

Previously we have studied the effect of the reduction of the mean ionic radius of A site in $Pr_{0.6}Sr_{0.4}MnO_3$ system with Na doping, on the magnetocaloric effect [13, 14]. In the present paper we extend the previous studies and report the structural and magnetocaloric properties of $Pr_{0.6}Sr_{0.4-x}K_xMnO_3$ (x= 0, 0.05, 0.1, 0.15 and 0.2) samples for which the Sr^{2+} ions are partially replaced with larger K^+ ions [15]. This in turn changes the Mn^{3+} / Mn^{4+} ratio and enhances the mean ionic radius of A-site. Temperature dependence of magnetic entropy change is analyzed by means of the so called universal curve [16-18]. An influence of applied magnetic field on the magnetic entropy change and relative cooling power are also discussed in order to assess potential application in magnetic refrigerating systems.

Experimental details

Powder samples $Pr_{0.6}Sr_{0.4-x}K_xMnO_3$ (x = 0, 0.05, 0.1, 0.15 and 0.2) were elaborated by the standard solid state reaction at high temperature. Stoichiometric ratio of Pr_6O_{11}, $SrCO_3$, K_2CO_3 and MnO_2 (99.9%) was mixed in an agate mortar and then heated in air to 1000°C for 60 h with intermediate grinding. The obtained mixtures were then pressed into pellets and sintered at 1100 °C in air for 60 h with intermediate grinding. Phase purity, homogeneity and cell parameters were studied by the X-ray diffraction with Cu-Kα radiation (1.54 Å) in the 2Θ range of 10 - 100 degrees. Structural analysis was carried out using the standard Rietveld technique [19, 20]. The morphology and grain size distribution were studied by SEM. The magnetic measurements of K doped manganites were carried out using ppms system in applied magnetic field up to 2 T and the undoped manganite was measured with vibrating sample magnetometer up to 7 T.

Structure

The room temperature X-ray diffraction patterns for x = 0.15 and 0.2 are shown in Fig. 1A-B. The remaining samples diffractograms (x = 0, 0.05 and 0.1) were reported separately [13, 21]. The diffractograms confirm that all $Pr_{0.6}Sr_{0.4-x}K_xMnO_3$ (x = 0 to 0.2) magnanites studied are a single phase with orthorhombic structure corresponding to the *Pnma* space group. No traces of any other secondary or impurity phase were detected. Structural parameters obtained by Rietveld analysis of the powder XRD data are listed in Table 1.

The unit cell parameters vary smoothly with potassium content x, as shown in Fig. 2A. It is worth to notice that the so called O' phase exists for all x values, as indicated by the relation $\frac{b}{a} \prec \sqrt{2}$ [22]. This is a signature of Jahn – Teller effect causing a distortion of MnO_6 octahedra, which removes the remaining degeneration. Potassium is observed to slightly increase the unit cell volume from 229.108 $Å^3$ for x = 0 to 229.295 $Å^3$ for x = 0.2 (Fig. 2B). Such a volume increase is caused by the considerable difference between the ionic radii of Sr^{2+} and K^+. For the ideal perovskite structure with 12-fold coordination of the A sites the ionic radii of Sr^{2+} and K^+ are equal to 1.44 Å and 1.64 Å, respectively [15]. On the other hand, the ionic radii are known to shrink gradually down to 1.18 Å and 1.38 Å for Sr^{2+} and K^+,

respectively, corresponding to the lowest six-fold coordination [15]. The more precise determination of ionic radii from the present structural data is not possible since the raising K doping level can modify both the lattice distortion and the local coordination. One may also notice the correlation between the mean ionic radius of the A site and the tolerance factor t, determined according to Shannon values [15] and with coordination 9, is varying from 0.9292 up to 0.9544, as seen in Tab. 1.

The average crystallite sizes of the prepared manganites are estimated by the Debye-Scherrer method, which considers a full width at half maximum of the most intense XRD peak. Tab. 1 shows the fine microstructure with average crystallite sizes (Cs) close to 50 nm for the studied K doped manganites.

The SEM images (Fig. 3A-D) show that the grains of manganites studied are irregularly spherical like and the mean sizes G_{SEM} are spread between 600 and 900 nm, which are slightly larger than those reported previously for $Pr_{0.6}Sr_{0.4-x}Na_xMnO_3$ (x = 0 to x =0.2) [13]. The agglomeration degree defined by the ratio G_{SEM} to crystallite size C_S [23] is about 16. This ratio confirms that the grains observed by SEM consist of multiple crystallites [24].

The average angle <Mn-O-Mn> was used to determine the tilt angle in the plane of the bond, which is an argument in cosine function in eq. 1. The average <Mn-O> bond length listed in the Tab. 1 is in turn used to determine the bandwidth W according to the following approximate formula [25, 26]:

$$W \propto \frac{\cos\frac{1}{2}\left(\Pi - \langle Mn - O - Mn \rangle\right)}{\left(d_{Mn-O}\right)^{3.5}} \qquad (1)$$

The W values are calculated with 0.01 accuracy and exhibit only a minute variation with K content. Tab. 1 shows that the Mn-O bond lengths diminish with raising x, which enhances the W values. It is hard to perform a very strict analysis, how the Mn-O-Mn angles affect W values since in contrast to monotonically varying Mn-O2-Mn angle the Mn-O1-Mn dependence on x is not monotonic (Tab. 1). However, one may speculate that the twice more populated Mn-O2-Mn angles, which grow with x, may be responsible for the minute suppression of W for x = 0.1 and perhaps 0.05 too.

Magnetic results

The magnetization was recorded during the heating run, after the sample was cooled down to the lowest temperature. The ZFC and FC magnetization curves split below the irreversibility temperature, which is about 15 K lower than the Curie temperature of manganites studied. As shown in typical plot for x= 0.2 sample in Fig. 4A, the FC branch increases with lowering of temperature, whereas a decreasing tendency is observed for the ZFC branch. The weak irregularity of ZFC and FC magnetization observed around 40 to 70 K and depending on potassium content, corresponds to an abrupt magnetization change in $Pr_{0.6}Sr_{0.4}MnO_3$ single crystal about 65 K [27, 28], which is caused by the structural transition from the high temperature orthorhombic P*nma* to the low temperature monoclinic I_2/a space group. This magnetization change shifts towards lower temperature for higher doping level. Its magnitude diminishes as the Mn^{3+} fraction is reduced.

The shape of the FC curves reveals the prevailing ferromagnetic ordering of magnetic moments, which may be partially induced by the magnetic field applied during the cooling of sample. On the contrary, the ZFC curve indicates the competition between the ferro- and antiferromagnetic interactions, which are of the double exchange and superexchange type, respectively. The relatively largest split between the FC and ZFC curves shows that the antiferromagnetic interactions are strongest for x = 0.2. The relatively broad distribution of competing interactions may be facilitated by the relatively high degree of structural disorder

present in the nanocrystalline materials as well as by the K doping. The similar behavior was reported for the akin manganite $Pr_{0.5}Sr_{0.2}M_{0.2}MnO_3$ (M = Na, Li, K and Ag) [10].

The temperature derivative of magnetization (Fig. 4B) was used to determine ferromagnetic Curie temperatures T_C. Values of T_C decrease gradually from 310 K for x = 0 [13] down to 269 K for x = 0.2 as a result of the decrease of effective exchange interaction when the Mn^{3+} fraction is reduced from 60 to 40 % with increasing K content.

An influence of the so called chemical pressure generated by e.g. potassium doping, is parameterized by means of the electronic bandwidth W, which may control the magnetic and transport processes in perovskites [25,26]. The W parameter has in fact the geometrical or structural nature being related to bond length and angles. Due to this limitation W neglects the distribution of the Mn^{3+} and Mn^{4+} ions over the B sites. The Mn^{3+} fraction decays from 0.6 down to 0.4 when K doping varies from 0 to 0.2 (Tab. 1) modifying the path of the motion of itinerant e_g electrons. This causes that the effective exchange interaction is reduced as revealed by decreasing values of T_C, despite the bandwidth W is only weakly oscillating.

The temperature dependence of the dc susceptibility $\chi(T)$ measured above T_C under a magnetic field of 0.01 T (not plotted) was checked to obey the Curie-Weiss law in the high temperature paramagnetic phase. The numerical fitting resulted in values of Curie Weiss temperatures θ and the effective magnetic moment (Tab. 2). One may notice that the potassium doping enhances the effective magnetic moment remarkably above 5.4 μ_B observed for x = 0 [13, 29]. The observed gradual decay of magnetic moment from 6.58 μ_B for x = 0.05 down to 6.43 μ_B for x = 0.2 is associated with Mn^{3+} (%) fraction diminishing from 0.6 to 0.4 for highest K content. One should also note that the obtained values are larger than the spin-only magnetic moments of 3.87 and 4.9 μ_B for Mn^{4+} and Mn^{3+}, respectively [30, 31]. It points to the additional contribution of magnetic Pr^{3+} ions bearing 3.5 μ_B [31, 32], which may enhance magnetic moment. One may also consider the polaron effect leading a formation of magnetic clusters [30].

The isothermal magnetization data registered in magnetic fields up to 7 T for x = 0 [13] and up to 2 T for x > 0 show that the magnetization M increases most abruptly in weak applied field (< 0.2 T) and then approaches to saturation for H > 1 T. Typical magnetization isotherms for x = 0.2 are shown in Fig. 5. The saturation magnetization increases with decreasing temperature and proves the typical ferromagnetic behavior of samples below the Curie temperature. An evolution in isotherm shape demonstrates a transition between the ferro- and paramagnetic phase of manganites studied. The similar behavior was reported for other manganites [13, 14]. The more detailed analysis of magnetization is impeded since the crystallite sizes of undoped manganite is smaller than crystallite sizes of the K doped manganites (Tab. 1). On the other hand, the grain sizes of K doped manganites are slightly larger as compared to Na doped ones with x = 0 to 0.2.

Due to the asymmetric shapes of the manganite samples the reliable demagnetization factors could not be ascribed and applied for calculation. Therefore, the Arrott plots are shifted towards higher H/M values. The Arrott plots, as shown for x = 0.2 sample in Fig. 6), deduced from isothermal magnetization confirms that all investigated samples exhibits a positive slope, which confirms the second order magnetic transition according to the Banerjee criterion [33]. The Curie temperatures derived from Arrott plots are close to those determined from low field magnetization measurements. (Arrott plot for x = 0 was reported in [13].)

Magnetic entropy

The magnetic entropy change ΔS, was calculated from isothermal magnetization measurements using thermodynamic Maxwell relation and the standard procedure described previously [13-14]. The ΔS values supply the characterization specific to the composition and microstructure of the material studied. The regular shape of magnetization isotherms as well

as of FC/ZFC curves, characteristic for ferromagnet, proves that the magnetic entropy change ΔS originates from single ferro- to paramagnetic phase transition. No trace of any, e.g. antiferromagnetic component with negative magnetic entropy change ΔS is seen in the whole temperature interval.

A typical temperature variation of magnetic entropy change at various magnetic fields for x = 0.2 sample plotted in Fig. 7 shows that the magnetocaloric effect in potassium doped manganites, attaining up to 3.2 J/kg K at 2 T depending on composition, is noticeably stronger as compared to 1.95 J/kg K found for the potassium free manganite $Pr_{0.6}Sr_{0.4}MnO_3$ [13]. The ΔS maximum is located in vicinity of Curie temperature. The width at a half maximum spreads up to about 30 K depending on composition. The K doping is found to be beneficial for magnetocaloric effect whereas for the Na doping into the same $Pr_{0.6}Sr_{0.4}MnO_3$ manganite the ΔS maximum did not exceed 1.84 J/kgK at 2 T magnetic field [13]. It is worth to notice that the lowest ΔS value is observed for x= 0.1 samples and is equal to 2.89 J/kgK.

The magnetic entropy change is known to depend both on temperature T and magnetic field B. This magnetic field dependence of maximum magnetic entropy change ΔS_{MAX} at Curie temperature T_C is usually approximated by the simple formula [17, 34]

$$\Delta S_{MAX}(H,T_C) = \text{const} \times H^{N(T)} \qquad (2)$$

The local N(T) exponent measures a sensitivity of magnetic entropy change to applied magnetic field [17,34]. The typical temperature variation of N(T) for various K doping level, derived from ΔS(H,T) data, is plotted in Fig. 8 for x = 0.2 sample. The ΔS(T) behavior is similar to that reported for the parent sample $Pr_{0.6}Sr_{0.4}MnO_3$ in previous works [13, 35]. At high temperature in the paramagnetic phase the N(T) values approach 2 due to the Curie - Weiss law [18]. With a decreasing temperature the N(T) minimum around Curie temperature T_C is followed by a slight increase of N(T) in ferromagnetic phase. The minimum N(T) values listed in Tab. 2 are very close to those found for other manganites [16] and transition metal based amorphous alloys (N = 0.75) [17]. Moreover, the gradual shift of N(T) curves towards lower values is observed with raising magnetic fields.

Universal curves of magnetic entropy change

The so called universal curves of magnetic entropy change were proposed and successfully applied as a simple tool to investigate the nature of magnetocaloric effect [17]. This approach was performed by normalizing the magnetic entropy change ΔS to its maximum value ΔS_{MAX} for each magnetic field change. The temperature axis was transformed according to the relation [17]

$$\Theta = -(T - T_C) / (T_{R1} - T_C) \quad \text{for } T < T_C \qquad (3)$$
$$\Theta = (T - TC) / (T_{R2} - T_C) \quad \text{for } T > T_C$$

The so called reference temperatures T_{R1} and T_{R2} correspond to the temperatures for which $\Delta S(T_{Ri}) = \Delta S_{MAX} / 2$.

The typical plots for transformed ΔS_M (T) curves for magnetic fields of 1 and 2 T are shown in Fig. 9 for the manganites studied. Moreover, Fig. 10 shows for $Pr_{0.6}Sr_{0.4}MnO_3$ that the experimental results merge into the universal curve for magnetic field up to 7 T. This behavior is distinctly different than that one typical for the first order phase transition [36] and proves that the manganites studied undergo the second order magnetic phase transition, which is consistent with the Arrott plots. One may notice that the second order transition was

reported for various fine structured manganites with mean crystallite sizes below around 100 nm [13, 35, 37, 38].

Cooling power

Among other parameters the ability of material for magnetocaloric refrigeration may be parameterized by the so called relative cooling power RCP, describing an amount of heat transported between temperatures corresponding to the half maximum width δT_{FWHM} . RCP is computed according to the following formula [39]:

$$RCP = - \Delta S_{MAX} * \delta T_{FWHM} \quad (4)$$

where ΔS_{MAX} is the maximum entropy change. The RCP values under a magnetic field of 2 T, listed in Tab. 2, show that the potassium doping causes a slight decrease of the RCP values as compared to 102 J/kg of the parent manganite $Pr_{0.6}Sr_{0.4}MnO_3$ [13]. This RCP reduction occurs due to the narrowed temperature interval δT, which for ΔB = 2 T shrinks from 52 K for undoped sample to about 30 K for K doped samples – compensating the ΔS_{MAX} enhancement. We should also note that RCP values are very comparable to those observed for $Pr_{0.6}Sr_{0.4-x}Na_xMnO_3$ manganites [13] exhibiting the roughly twice broader temperature half width accompanied by the reduced ΔS_{MAX}. Among the K doped manganites the highest RCP of 95.6 J/kg is observed for x = 0.05 whereas the lowest value of 83 J/kg appears for x= 0.1. The slightly lower RCP = 92 J/kg is observed for $Pr_{0.6}Sr_{0.35}Na_{0.05}MnO_3$ manganite [14]. One may note that RCP does not evolve regularly, as was observed for Na doped manganites [13]. Such a behavior can be related to the strong sensitivity of RCP to the microstructure created during various preparation and treatment processes. This pertains mainly the grain sizes of present samples, which are slightly larger than those reported for sodium series [13, 14]. The RCP values of K doped manganites studied are considerably higher than those 58.9, 59.3, 69.6 and 54.6 J/kg reported for samples $Pr_{0.5}Sr_{0.3}M_{0.2}MnO_3$ doped with M = Na, Li, K and Ag, respectively [10,11].

Some uncertainty may arise concerning the magnetocaloric parameters originating from measurements registered with different temperature steps. A simple analysis, how the temperature step affects the ΔS, ΔS_{MAX} and δT_{FWHM} values, may suggest the optimum condition, when a number of experimental points between e.g. $\Delta S_{MAX}/2$ values is approximately the same for the compared samples. This condition practically facilitates and justifies a comparison of magnetocaloric parameters for the relatively narrow or broad phase transitions.

The influence of magnetic field on RCP may be estimated according to the formula [13,40]:

$$RCP(H) = \text{const } H^R \quad (5)$$

The R exponents obtained from the numerical fit of RCP are listed in Tab. 2 with accuracy about 0.02 for each composition. The K doping enhances R exponent from 1.04 for undoped manganite to 1.22 for x equal to 0.05 and 0.1. Gradual reduction in R is seen for x > 0.1. These R results are compatible with values previously reported for Na doped manganites [13] and those observed for amorphous metallic alloys (R = 1.15) by Franco [41].

Conclusions

The structural study of $Pr_{0.6}Sr_{0.4-x}K_xMnO_3$ manganites reveals that it has orthorhombic structure with Pnma space group with mean grain size varying from 600 to 900 nm. The exchange interaction is weakened by the increasing K content, which shifts the Curie

temperature from 310 K for x = 0 down to 269 K for x = 0.2. The maximum magnetic entropy change under magnetic field variation of 2 T is found to be 1.95, 3.09, 2.89, 3.05 and 3.2 J/kgK, respectively, for K content x varying from 0 to 0.2. The resulting relative cooling power has a maximum of 102 J/kg for x= 0. The same RCP value is also reported for the similar manganite $Pr_{0.63}Sr_{0.37}MnO_3$ [42]. The enhanced magnetic entropy change in K doped manganites is accompanied by a reduction in temperature half width, which suppresses RCP below 102 J/kg. A sensitivity of magnetic entropy change to magnetic field is estimated by a local N(T) exponent exhibiting the characteristic temperature variation. The universal curves of entropy change and Arrott plots confirm the second order phase transition. The RCP dependence on magnetic field is comparable with that reported for Na doped manganites [13]. The above experimental testing shows that K doping enables to tailor the Curie temperature but slightly reduces the cooling power of manganites studied.

Acknowledgements. This work was supported in parts by the Tunisian Ministry of Higher Education and Scientific Research and by Ministry of Science and Higher Education (Poland) and WBI (Belgium) in a frame of scientific exchange agreement.

References

[1] S.V. Trukhanov, L.S. Lobanovski, M.V. Bushinsky, I.O. Troyanchuk, H. Szymczak, J. Phys. Condens. Matter 15 (2003) 1783.
[2] C. Zener, Phys. Rev. 81 (1951) 440.
[3] C. Zener, Phys. Rev. 82 (1951) 403.
[4] A.J. Millis, P.B. Littlewood, B.I. Shraiman, Phys. Rev. Lett. 74 (1995) 5144.
[5] J.B. Goodenough, Phys. Rev. 100 (1995) 564
[6] V. Suresh Kumar, R. Mahendiran, Solid State Comm. 150 (2010) 1445
[7] V. S. Kolat, T. Izgi, A.O. Kaya, N. Bayri, H. Gencer, S. Atalay, J. Magn. Magn. Mater. 322 (2010) 427.
[8] A. G. Gamzatov, A. B. Batdalov, Physics of the Solid State, 54 (2012) 70.
[9] S. Roy, Y. Q. Guo, S. Venkatesh and N. Ali, J. Phys.: Condens. Matter 13 (2001) 9547
[10] H. Yang, P. Zhang, Q. Wu, H. Ge, M. Pan, Journal of Magnetism and Magnetic Materials 324 (2012) 3727.
[11] T. Tang, K.M. Gu, Q.Q. Cao, D.H. Wang, S.Y. Zhang, Y.W. Du, Journal of Magnetism and Magnetic Materials 222 (2000) 110
[12] J. Hejtmanek, Z. Jirak, J. Sebek, A. Strejc, Journal of Applied Physics 89 (2001) 7413
[13] R. Thaljaoui, W. Boujelben, M. Pękała, K. Pękała, W. Cheikhrouhou-Koubaa, A. Cheikhrouhou, J. Mater. Sci. 48 (2013) 3894
[14] R. Thaljaoui, W. Boujelben, M. Pękała, D. Pociecha, J. Szydłowska, A. Cheikhrouhou, J. Alloys Compounds 530 (2012) 138.
[15] R.D. Shannon, Acta Cryst. A 32 (1976) 751.
[16] M. Pękała, Journal of Applied Physics 108 (2010) 113913
[17] V. Franco, A. Conde, J. M. Romero-Enrique and J. S. Blázquez J. Phys. Cond. Matter 20 (2008) 285207
[18] R. Szymczak, R. Kolano, A. Kolano-Burian, V.P. Dyakonov, H. Szymczak, Acta Physica Polonica 117 (2010) 203
[19] H.M. Rietveld, J. Appl. Cryst. 2 (1969) 65
[20] T. Roisnel, J. Rodriguez-Carvajal, Computer program FULLPROF, LLB-LCSIM. May 2003.
[21] R. Thaljaoui, W. Boujelben, M. Pękała, A. Cheikhrouhou, J. Supercond Nov Magn 26 (2013) 1625

[22] K. Knížek, Z. Jirák, E. Pollert, F. Zounová, S. Vratislav, J. Solid State Chem. 100 (1992) 292
[23] M. Soleymani, A. Moheb, E. Joudaki, Central Eur. J. Chem. 7 (2009) 809.
[24] S. Das, T.K. Dey, J. Phys. D: Appl. Phys. 40 (2007) 185.
[25] P.G. Radaelli, G. Iannone, M. Marezio, H.Y. Hwang, S.-W. Cheong, J.D. Jorgensen, D.N. Argyriou, Phys. Rev. B 56 (1997) 8265.
[26] M. Medarde, J. Mesot, P. Lacorre, S. Rosenkranz, P. Fisher, K. Gobrecht, Phys. Rev. B 52 (1995) 9248.
[27] S. Roessler, Harikrishnan S. Nair, U. K. Roessler, C.M.N. Kumar, Suja Elizabeth, and S. Wirth, Phys. Rev. B 84 (2011) 184422.
[28] W. Boujelben, M. Ellouze, A. Cheikh-Rouhou, J. Pierre, Q. Cai, W.B. Yelon, K. Shimizu, C. Dubourdieu, Journal of Alloys and Compounds 334 (2002) 1
[29] S. Zemni, M. Baazaoui, Ja. Dhahri, H. Vincent, M. Oumezzine, Materials Letters 63 (2009) 489
[30] V. Dyakonov, A. Ślawska-Waniewska, J. Kaźmierczak, K. Piotrowski, O. Iesenchuk, H. Szymczak, E. Zubov, S. Myronova, V. Pashchenko, A. Pashchenko, A. Shemjakov, V. Varyukhin, S. Prilipko, V. Mikhaylov, Z. Kravchenko, A. Szytuła, W. Bażela Low Temperature Physics 35 (2009) 568
[31] J.M.D. Coey, Magnetism and Magnetic Materials, Cambridge Un. Press, 2010
[32] A.H. Morrish, The Physical Principles of Magnetism, Wiley 1965.
[33] S.K. Banerjee, Phys. Lett. 12 (1964) 67
[34] M. Pękała, K. Pękała, V. Drozd, K. Staszkiewicz, J.-F. Fagnard, P. Vanderbemden, Journal of Applied Physics 112 (2012) 023906
[35] R. Thaljaoui, W. Boujelben, M. Pękała, K. Pękała, J. Mucha, A. Cheikhrouhou, J. Alloys Compds 558 (2013) 236
[36] C. M. Bonila, J. H. Albillos, F. Bartolome, L. M. Garcia, M. P. Borderias, V. Franco, Phys. Rev. B 81 (2010) 224424.
[37] A. Tozri, E. Dhahri, E.K. Hlil, M. Sajieddine, M. Valente, PIERS Proceedings, Marrakesh, MOROCCO, March 20-23, 2011
[38] M.H. Phan, S.-C. Yu, J. Magn. Magn. Mat. 308 (2007) 325
[39] A.M. Tishin, Y.I. Spichkin, The Magnetocaloric effect and its Applications, IoP Publishing, Bristol and Philadelphia, 2003
[40] V. Franco, J.S. Blazquez, B. Ingale, A. Conde, Annu. Rev. Mater. Sci. 42 (2012) 305
[41] V. Franco, J.S. Blázquez, A. Conde, J. Appl. Phys. 103 (2008) 07B316.
[42] M.H. Phan, H.X. Peng, S.C. Yu, J. Appl. Phys. 97 (2005) 10M306

Figures

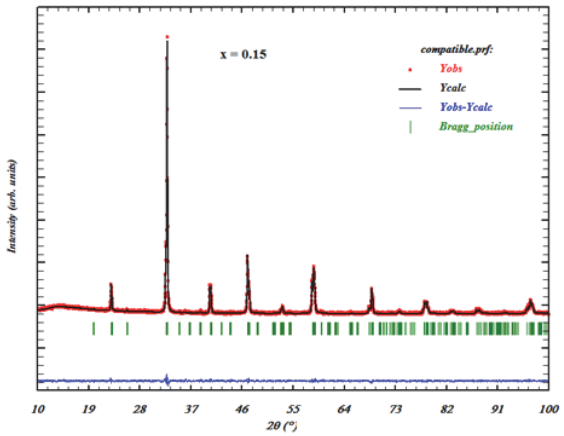

Fig. 1 A

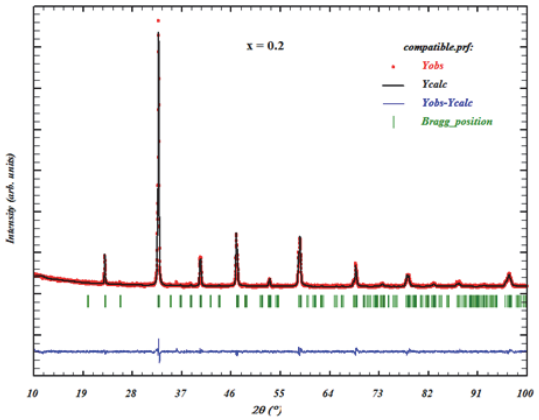

Fig. 1B

Fig. 1. XRD patterns for $Pr_{0.6}Sr_{0.4-x}K_xMnO_3$ manganites with x = 0.15 (A) and 0.2 (B).

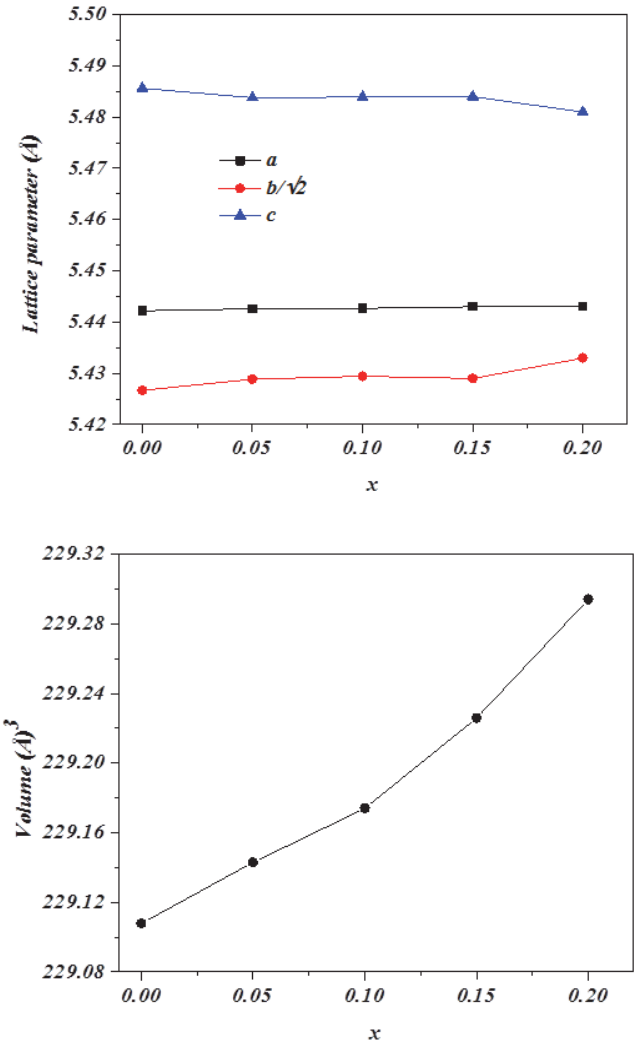

Fig. 2. Variation of unit cell parameters (A) and volume (B) as a function of K content x.

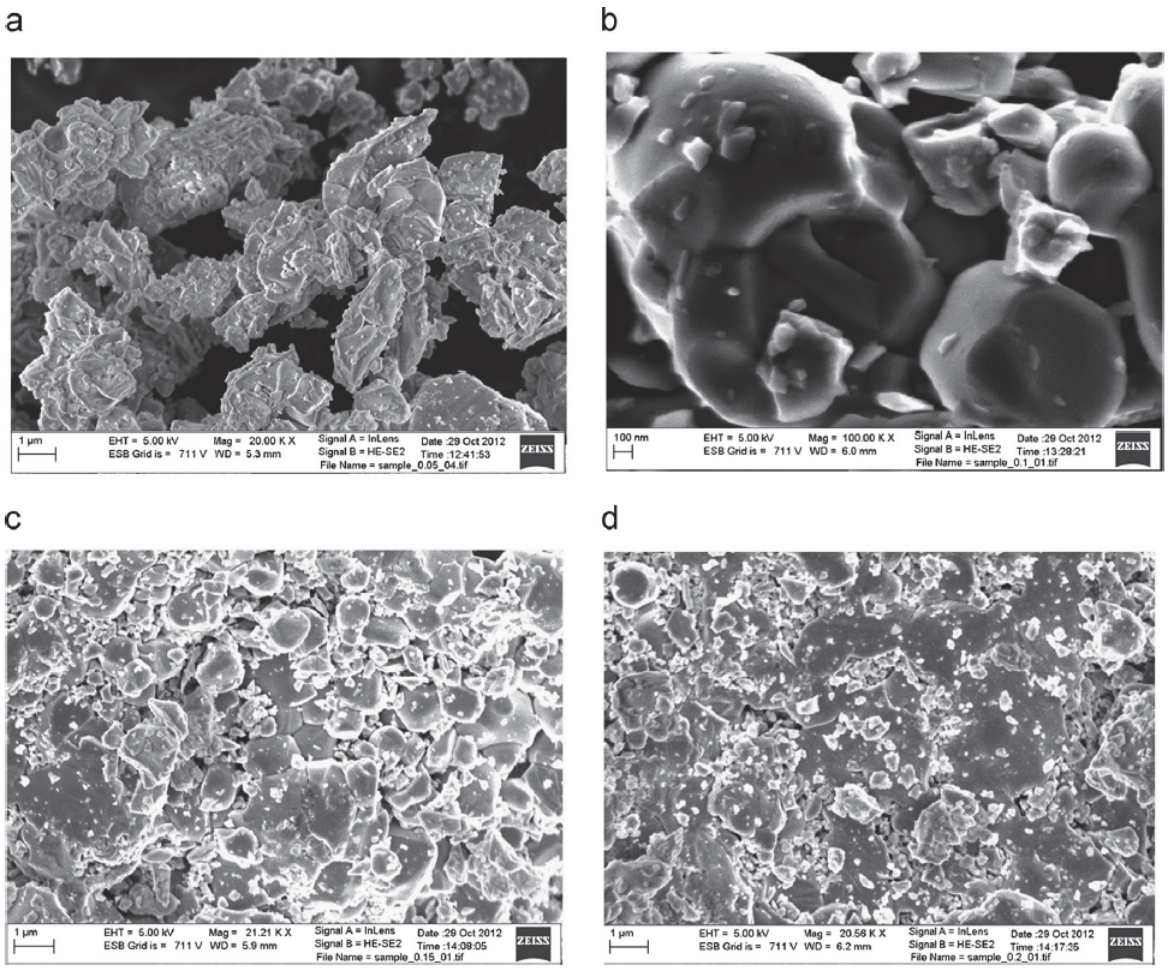

Fig. 3. Scanning electron micrograph of $Pr_{0.6}Sr_{0.4-x}K_xMnO_3$ manganites for x = 0.05 to 0.2 (A to D).

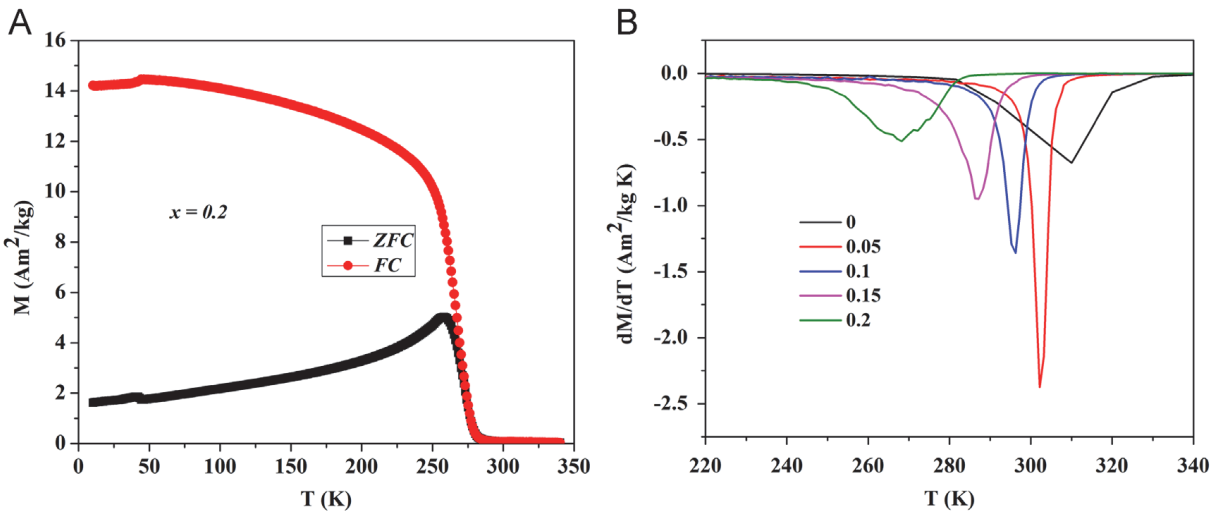

Fig. 4. Temperature variation of zero field cooled (ZFC) and field cooled ((FC) magnetization measured at magnetic field of 100 Oe for $Pr_{0.6}Sr_{0.2}K_{0.2}MnO_3$ manganite (A) and temperature derivative of magnetization for x = 0 to 0.2 (B).

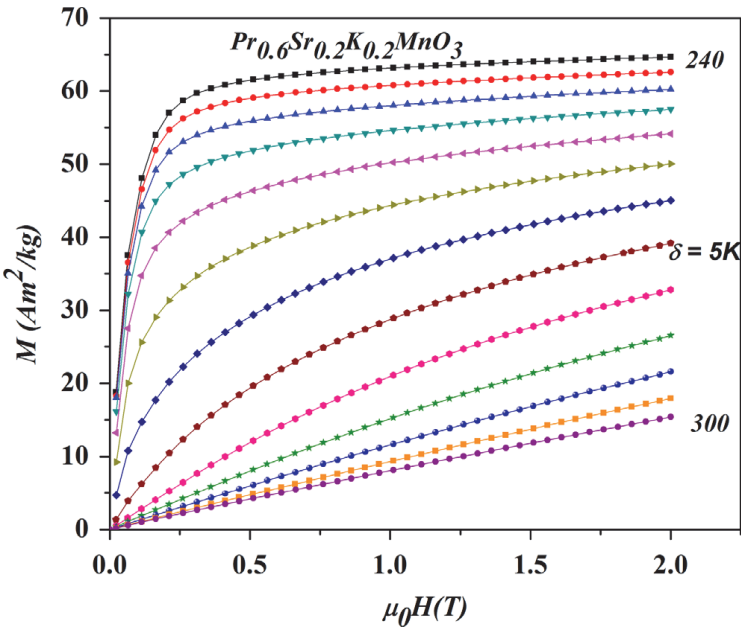

Fig. 5. Magnetization isotherms for $Pr_{0.6}Sr_{0.2}K_{0.2}MnO_3$ manganite.

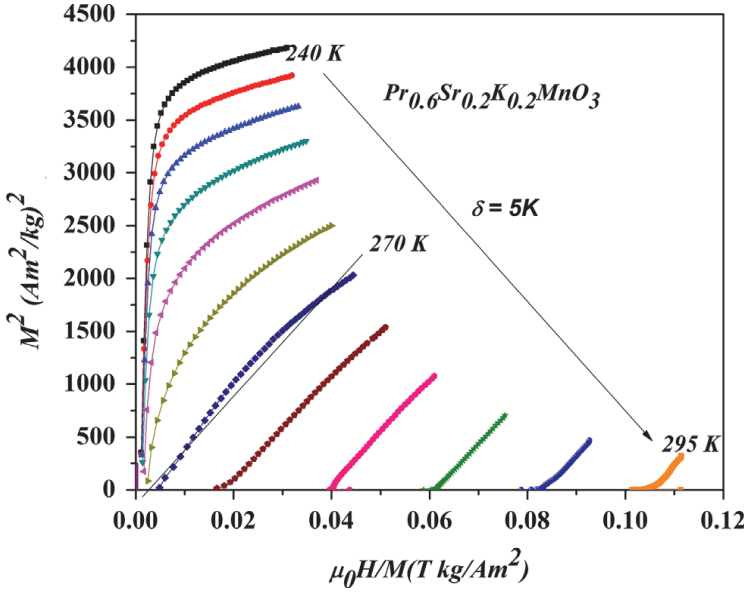

Fig. 6. Arrott plots for $Pr_{0.6}Sr_{0.2}K_{0.2}MnO_3$ manganite.

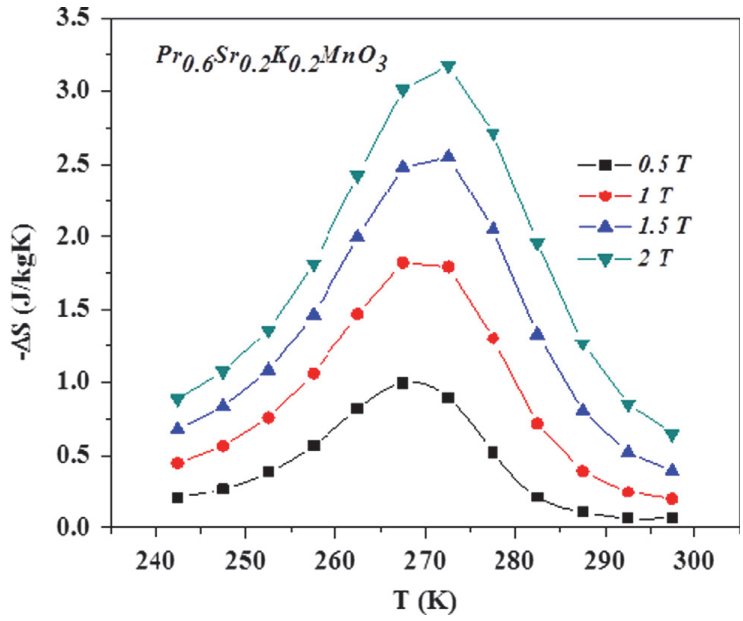

Fig. 7. Temperature variation of magnetic entropy change at various magnetic field change for $Pr_{0.6}Sr_{0.2}K_{0.2}MnO_3$ manganite.

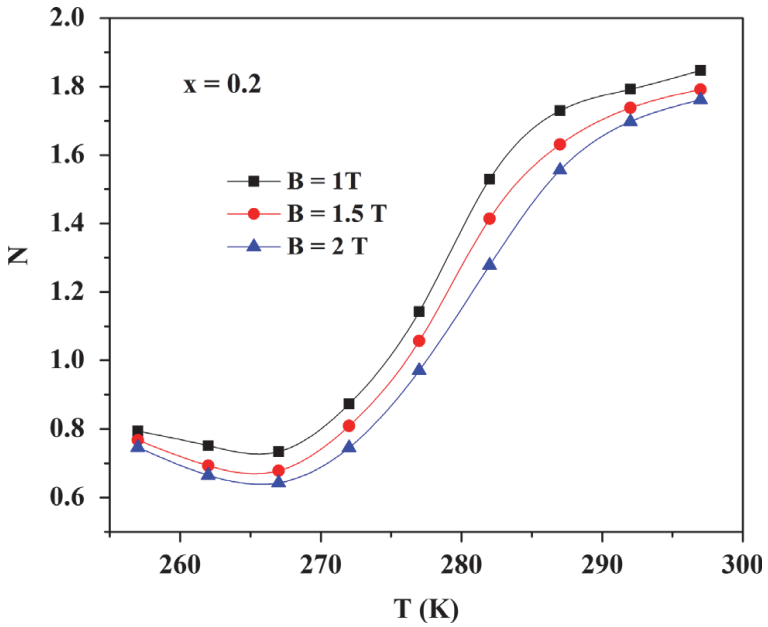

Fig. 8. Temperature dependence of the local exponent N(T) at magnetic fields of 1, 1.5 and 2 T for $Pr_{0.6}Sr_{0.2}K_{0.2}MnO_3$ manganite.

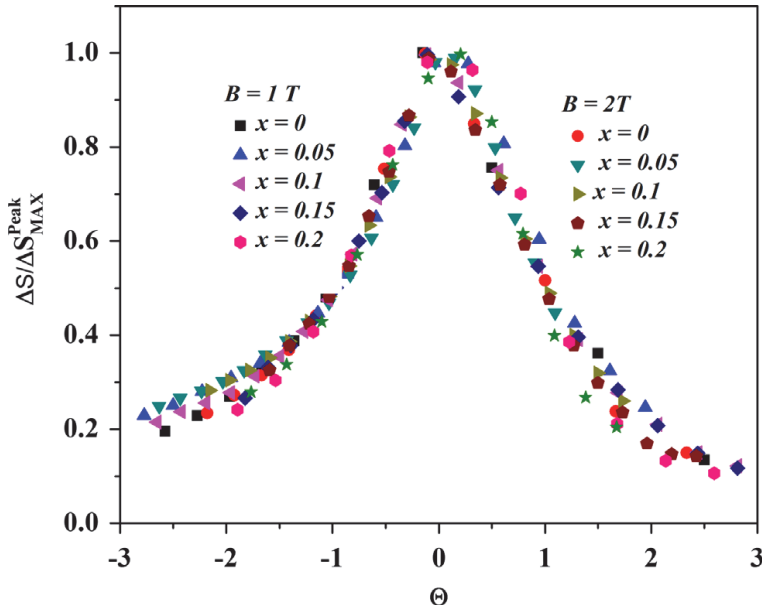

Fig. 9. Universal curve of magnetic entropy change at B = 1 and 2 T for x = 0.05 to 0.2.

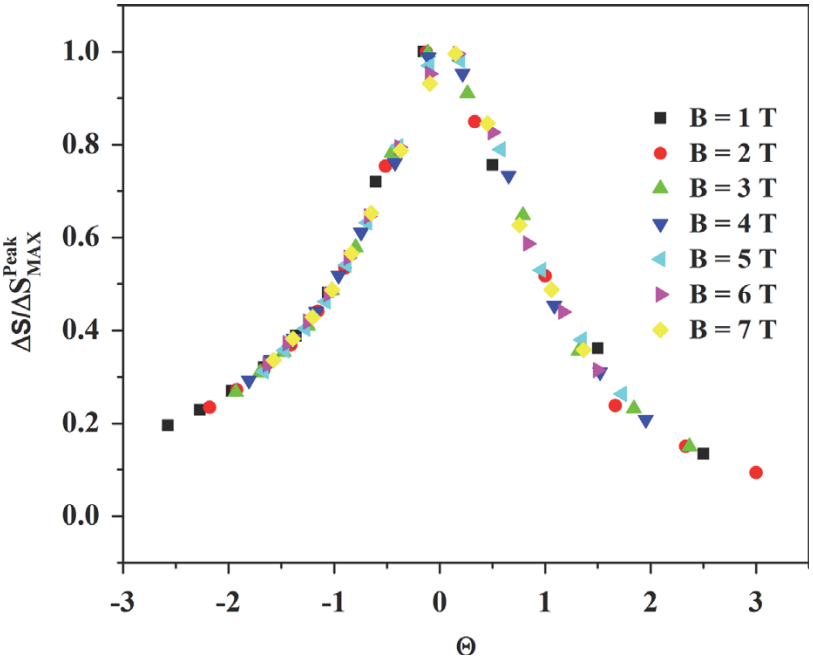

Fig. 10. Universal curve of magnetic entropy change for x = 0 up to B = 7 T for x = 0.

Table 1. Structural data for $Pr_{0.6}Sr_{0.4-x}K_xMnO_3$ manganites.

$Pr_{0.6}Sr_{0.4-x}K_xMnO_3$	x = 0	x = 0.05	x = 0.1	x = 0.15	x = 0.2
a (Å)	5.4422(8)	5.4421(6)	5.4427(3)	5.4434(3)	5.4437(3)
b (Å)	7.6744(1)	7.6772(5)	7.6783(4)	7.6784(4)	7.6848(4)
c (Å)	5.4856(8)	5.4831(8)	5.4839(3)	5.4844(3)	5.4811(2)
V(Å^3)	229.108(1)	229.143(2)	229.17(2)	229.23(2)	229.295(2)
Mn-O1 (Å)	1.948(5)	1.947(6)	1.946(9)	1.938(6)	1.948(6)
Mn-O2 (Å)	1.984(8)	1.967(1)	1.961(2)	1.931(7)	1.931(2)
Mn-O1-Mn(°)	159.8(8)	161.8(1)	161.8(8)	161.3(4)	160.9(3)
Mn-O2-Mn(°)	162.9(4)	163.3(1)	163.8(3)	164.3(3)	165.2(1)
t	0.9292	0.9352	0.9416	0.9480	0.9544
$\langle r_A \rangle$ (Å)	1.226	1.232	1.253	1.262	1.274
W	0.097	0.095	0.094	0.096	0.097
Cs (nm)	41	49	52	54	51

Table 2. Magnetic parameters for $Pr_{0.6}Sr_{0.4-x}K_xMnO_3$ manganites.

$Pr_{0.6}Sr_{0.4x}K_xMnO_3$	x= 0	x= 0.05	x = 0.1	x = 0.15	x= 0.2
Mn^{3+}(%)	60	55	50	45	40
T_C (K)	310	301	296	287	269
Θ (K)	312	303	295	284	275
μ_{eff} (μ_B)	5.4	6.58	6.47	6.45	6.43
ΔS_{MAX}($Jkg^{-1}K^{-1}$) at 2T	1.95	3.09	2.89	3.05	3.2
RCP (Jkg^{-1}) at 2T	102	95.6	83.8	85.4	92.8
N at T_C at 2 T	0.72	0.75	0.8	0.77	0.84
R	1.04	1.22	1.22	1.09	1.04